International Journal of Pharmaceutics 657 (2024) 124161

Contents lists available at ScienceDirect

International Journal of Pharmaceutics

journal homepage: www.elsevier.com/locate/ijpharm

Powder bed fusion–laser beam (PBF-LB) three-dimensional (3D) printing: Influence of laser hatching distance on the properties of zolpidem tartrate tablets

Ivana Adamov [a], Gordana Stanojević [b], Stefan M. Pavlović [c], Djordje Medarević [a], Branka Ivković [d], David Kočović [b], Svetlana Ibrić [a,*]

[a] Department of Pharmaceutical Technology and Cosmetology, Faculty of Pharmacy, University of Belgrade, Vojvode Stepe 450 11221, Belgrade, Serbia
[b] Institute for Medicines and Medical Devices of Montenegro, Ivana Crnojevića 64a 81000, Podgorica, Montenegro
[c] Institute of Chemistry, National Institute of Republic of Serbia, Technology and Metallurgy, University of Belgrade, Njegoševa 12 11000, Belgrade, Serbia
[d] Department of Pharmaceutical Chemistry, Faculty of Pharmacy, University of Belgrade, Vojvode Stepe 450 11221, Belgrade, Serbia

ARTICLE INFO

Keywords:
additive manufacturing
printed medicines
laser sintering
tablet morphology
drug dissolution rate
individualization of therapy

ABSTRACT

Laser sintering, known as powder bed fusion–laser beam (PBF-LB), offers promising potential for the fabrication of patient-specific drugs. The aim of this study was to provide an insight into the PBF-LB process with regard to the process parameters, in particular the laser hatching distance, and its influence on the properties of zolpidem tartrate (ZT) tablets. PHARMACOAT® 603 was used as the polymer, while Candurin® Gold Sheen and AEROSIL® 200 were added to facilitate 3D printing. The particle size distribution of the powder blend showed that the layer height should be set to 100 μm, while the laser hatching distance was varied in five different steps (50, 100, 150, 200 and 250 μm), keeping the temperature and laser scanning speed constant. Increasing the laser hatching distance and decreasing the laser energy input led to a decrease in the colour intensity, mass, density and hardness of the ZT tablets, while the disintegration and dissolution rate were faster due to the more fragile bonds between the particles. The laser hatching distance also influenced the ZT dosage, indicating the importance of this process parameter in the production of presonalized drugs. The absence of drug-polymer interactions and the amorphization of the ZT were confirmed.

1. Introduction

Over the last decade, many efforts have been made to explore three-dimensional (3D) printing and its potential for the production of pharmaceutical dosage forms (Lim et al., 2018; Trenfield et al., 2019). Since the approval of Spritam® in 2015 (Aprecia Pharmaceuticals, USA), no new drug has come to market that has been manufactured using 3D printing, but a new perspective for drug development and manufacturing has emerged (Souto et al., 2019). Since the introduction of the concept of precision medicine, a paradigm shift from large-scale drug manufacturing to the production of small manufacturing lots of drugs specifically tailored to the needs of individual patients has taken a major role in the field of drug discovery and development. 3D printing is an additive manufacturing (AM) process in which materials are successfully bonded together to create physical objects according to the specifications of 3D model data (ISO/ASTM DIS 52910(en), n.d.). It has been recognised that 3D printing as an AM process can play an important role in the delivery of patient-specific medicines (Gueche et al., 2021). 3D printing can contribute to more precise dosing and mitigate the adverse effects of drugs. In addition, the most desirable therapeutic outcomes could be achieved (Stanojević et al., 2020; Gueche et al., 2021). Therefore, many AM technologies are being intensively researched to capitalise on all the advantages that these technologies could offer in the field of so-called printed drugs (Palo et al., 2017; Wang et al., 2021; Gaurav et al., 2021).

Based on the American Society for Testing and Materials (ASTM) International, the numerous 3D printing technologies have been categorised into seven categories: binder jetting, vat polymerisation,

* Corresponding author at: Department of Pharmaceutical Technology and Cosmetology, Faculty of Pharmacy, University of Belgrade, Vojvode Stepe 450 11221, Belgrade, Serbia.
E-mail addresses: ivana.adamov@pharmacy.bg.ac.rs (I. Adamov), gordana.boljevicstanojevic@cinmed.me (G. Stanojević), stefan.pavlovic@ihtm.bg.ac.rs (S.M. Pavlović), branka.ivkovic@pharmacy.bg.ac.rs (B. Ivković), svetlana.ibric@pharmacy.bg.ac.rs (S. Ibrić).

https://doi.org/10.1016/j.ijpharm.2024.124161
Received 8 March 2024; Received in revised form 22 April 2024; Accepted 22 April 2024
Available online 25 April 2024

powder bed fusion, material extrusion, material jetting, directed energy deposition and sheet lamination (ISO/ASTM DIS 52910(en), n.d.). Among them, laser sintering (LS), also known as powder bed fusion–laser beam (PBF-LB) is one of the latest processes introduced in the pharmaceutical field. According to the standard terminology, PBF-LB was formerly known as selective laser sintering (SLS) (ISO/ASTM DIS 52910(en), n.d.). This technology is characterised by the selective fusion of a material in which the thermal energy of a laser beam forms a solid part according to the well-known layer-on-layer mechanism (ISO/ASTM DIS 5 (2910)(en), n.d). In this single-step process, the feedstock in the form of powder is homogeneously distributed in a powder bed using a roller, while the laser is focused according to the data of the 3D model to draw specific patterns on the powder surface. The result is a fusion of the powder and the formation of solid bonds between the particles. Once the first layer has been successfully fabricated, the powder bed (build chamber) moves downwards while the feed region (reservoir chamber) moves upwards. A new layer of fresh powder is then deposited on top of the previous layer and the process is repeated until the complete part is fabricated (Allahham et al., 2020). A schematic representation of the PBF-LB printing process can be found in Fig. 1.

PBF-LB as an AM process offers many advantages, such as high resolution, the possibility of recycling the powder, the absence of post-processing and the possibility of fabricating parts with high porosity (Gueche et al., 2021). Powder excipients, which are usually used in conventional manufacturing processes such as direct compression, are also used in the PBF-LB process. The use of pharmaceutically safe powder excipients makes the PBF-LB a "safe" process that combines innovative and traditional approaches to drug manufacturing (Gueche et al., 2021). In the pharmaceutical field, PBF-LB has been used to produce various types of pharmaceutical dosage forms, e.g. multi-drug miniprintlets loaded with paracetamol and ibuprofen (Awad et al., 2019), orally disintegrating tablets (Fina et al., 2018a; Allahham et al., 2020), multidrug films (Kopp et al., 2023) and also drug delivery devices (Cheah et al., 2002; Leong et al., 2006). Nevertheless, complex structures for drug delivery, such as paracetamol gyroid lattice printlets^{TM}, have also been successfully produced using this 3D printing technology (Fina et al., 2018b). Modified and/or controlled release matrices manufactured using PBF-LB have also been proposed in several studies, including high-dose 3D printed dosage forms (Kulinowski et al., 2021; Yang et al., 2021; Kulinowski et al., 2022).

The powder bed fusion process itself must be optimised if different dosage forms are to be produced. Since drug printing using this technology has only recently attracted the attention of researchers, in the absence of a clear guideline, the principle of trial and error is usually applied to determine various process parameters and obtain dosage forms with suitable physicochemical properties (Madžarević et al., 2021). Nevertheless, artificial intelligence tools, such as machine learning, have recently been investigated as an alternative to the traditional trial-and-error approach in optimising numerous parameters in the PBF-LB process (Abdalla et al., 2023). Of the process parameters, the influence of laser scanning speed, temperature and layer height on the properties of the produced dosage forms has been reported in the literature, while the influence of the scanning distance, also referred to in the literature as laser hatching distance or hatch spacing, has not yet been studied in such detail (Fina et al., 2018a; Barakh Ali et al., 2019; Awad et al., 2020; Kulinowski et al., 2021; Madžarević et al., 2021; Trenfield et al., 2022). The laser hatching distance, which represents the distance between the centres of two consecutive laser beams, and its effects on high-dose controlled-release dosage forms have so far only been investigated by Kulinowski et al. (2021).

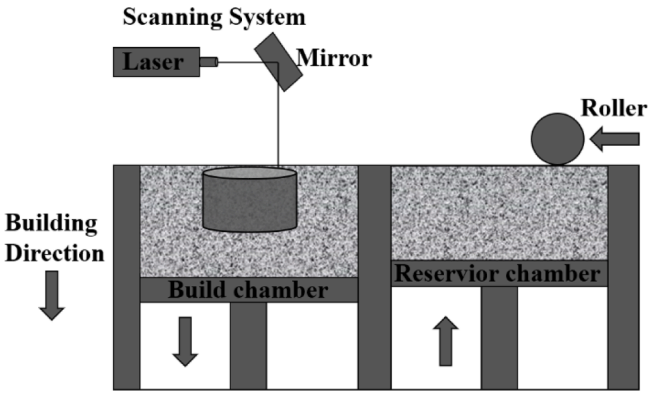

Fig. 1. Schematic representation of the PBF-LB process.

The aim of this study was therefore to investigate the influence of laser hatching distance on the properties of zolpidem tartrate tablets fabricated using PBF-LB 3D printing technology and to contribute to a better understanding of the powder bed fusion process in the manufacture of dose-adjusted drugs. With regard to so-called dose tailoring, zolpidem tartrate, a short-acting hypnotic (Sweetman, 2009), was selected as a suitable model drug that requires individualisation of therapy, such as gender- and age-appropriate dosing regimens (Adamov et al., 2022), including withdrawal therapy, which is usually required because the efficacy of benzodiazepines decreases over time, while side effects predominate (Henry et al., 2021). Therefore, the development of a flexible dosing platform to support appropriate and safe use of zolpidem tartrate may be of paramount importance.

2. Material and methods

2.1. Material

The zolpidem tartrate (ZT, MW 764.88 g/mol) used as model drug was kindly provided by Hemofarm AD, Vršac, Serbia, while the polymer PHARMACOAT® 603 (hydroxypropyl methylcellulose, HPMC, substitution type 2910, MW 16,000 g/mol) was kindly provided by Shin-Etsu Chemical Co, Ltd, Tokyo, Japan. Candurin® Gold Sheen, a gold pigment, was provided by Merck, Darmstadt, Germany, and AEROSIL® 200 (colloidal silicon dioxide) was provided by Evonik, Essen, Germany. All other chemicals used in the study were of analytical grade.

2.2. Powder preparation

150 g of the pharmaceutical powder blend (hereinafter referred to as F603 powder blend) was prepared by mixing 5 % (w/w) ZT, 91.5 % (w/w) PHARMACOAT® 603, 3 % (w/w) Candurin® Gold Sheen and 0.5 % (w/w) AEROSIL® 200 in a mortar and pestle. Since the particle size has been shown to be a critical parameter for the optimal flowability of the powder blends as a feedstock and thus a key factor for a successful powder bed fusion process (Goodridge et al., 2012), the prepared powder mixture was sieved through the 125 μm sieve in the next step and thoroughly mixed again. The composition of the prepared powder mixture is listed in Table 1.

2.3. Characterisation of pharmaceutical powder blend

2.3.1. Particle size distribution

Particle size analysis was performed using a laser diffraction analyser, the Malvern® Mastersizer 2000 (Malvern Instruments Ltd., UK), equipped with a Scirocco 2000 module for dry measurements. A small amount of the F603 powder blend was dispersed in air at a pressure of 0.5 bar. The particle size distribution (PSD) was characterised by the cumulative d_{10}, d_{50} and d_{90} particle undersize values.

Table 1
The composition (% w/w) of the pharmaceutical powder blend.

Formulation	ZT	HPMC	Candurin® Gold Sheen	AEROSIL® 200
F603	5.0	91.5	3.0	0.5

2.3.2. Powder flow properties

The flowability of the F603 powder blend was determined both by the direct method, using the GDT flowmeter (Erweka GmbH, Heusenstamm, Germany), and by the indirect method. The time required for 20 g of the sample to flow through the funnel of the device was measured and the results were expressed as mass flow rate (g s^{-1}). Measurements were performed in triplicate. Bulk density (ρ_{bulk}) and tapped density (ρ_{tapped}) were determined in triplicate with a 50 mL graduated cylinder using 20 g of sample and a STAV 2003 shaking volumeter (J. Engelsmann AG, Ludwigshafen, Germany). The corresponding volume was read to the nearest graduated unit after 1250 shaking cycles. The compressibility index and Hausner ratio were then calculated according to equations (1) and (2):

$$Compressibility\ index(\%) = 100 \times \left(\rho_{tapped} - \rho_{bulk}\right)/\rho_{tapped} \quad (1)$$

$$Hausner\ Ratio = \rho_{tapped}/\rho_{bulk} \quad (2)$$

The flowability properties were determined according to the descriptive terms in Ph. Eur. 11.0 (2.9.36. Powder flow).

2.4. 3D printing

Autodesk Fusion 360 software version 2.0.8809 (Autodesk Inc., San Rafael, CA, USA) was used to design the templates of the cylindrical tablets (10.00 mm diameter × 3.00 mm height). The 3D model data was exported as an STL file to the 3D printer software Sintratec version 1.2.0. The prepared F603 powder blend was transferred to the modified powder container of the 3D printer (Sintratec Kit, AG, Brugg, Switzerland), which is equipped with a 2.3 W 455 nm laser. The modification of the powder container was carried out to permanently reduce the volume of the chambers and the amount of powder required for the 3D printing process, while all other performances of the device itself were not changed. The modification made has no impact on the laser scanning system and the 3D printing process of dosage forms in general.

In the absence of suitable guidelines in the literature, initial experiments were carried out to optimise the powder bed fusion process according to the principle of trial and error. Chamber and surface temperature as well as the laser scanning speed were varied in different ranges, while the laser hatching distance was kept constant at five different levels (50 μm, 100 μm, 150 μm, 200 μm and 250 μm) until the optimal process parameters were determined. All other parameters were left at the default values, including the layer height. The default value for the layer height set by the 3D printer software is 100 μm and was not changed based on the previously obtained results for the characterisation of the prepared powder mixture. In accordance with the results of these experiments, the tablets were fabricated with the process parameters listed in Table 2.

2.5. Physical and mechanical properties of the tablets

2.5.1. Tablet morphology

The diameter and thickness of the tablets ($n = 10$) were measured using a digital caliper (Vogel Germany GmbH & Co. KG, Kevelaer, Germany). Images were taken with a Xiaomi Mi 11i camera.

Table 2
Experimental parameters of PBF-LB for the fabrication of tablets.

Formulation	Chamber Temperature (°C)	Surface Temperature (°C)	Laser Scanning Speed (mm s^{-1})	Layer Height (μm)	Laser Hatching Distance (μm)
F603 50	130	150	250	100	50
F603 100	130	150	250	100	100
F603 150	130	150	250	100	150
F603 200	130	150	250	100	200
F603 250	130	150	250	100	250

2.5.2. Weight variation

Fabricated tablets were weighed using a weighing boat and a calibrated balance (Kern & Sohn, Germany). The average weight and standard deviation for the tablets were calculated ($n = 10$).

2.5.3. Tablet density

The height and diameter of each tablet ($n = 10$) were measured at three different points where the average was recorded. The theoretical tablet volume was calculated using Eq. (3), to describe the volume of the cylinder:

$$V = \pi r^2 \times h \quad (3)$$

where V = tablet volume, r = radius and h = height.

The theoretical density of the tablets was then calculated according to Eq. (4):

$$\rho = m/V \quad (4)$$

where ρ = tablet density, m = mass and V = volume.

2.5.4. Mercury intrusion porosimetry (MIP)

The MIP measurements were performed with the fully automated conventional Carlo Erba Porosimeter 2000 (pressure range: 0.1–200 MPa; pores with a diameter between 7.5 and 15,000 nm). The analysis data was recorded using Milestone Software 200. Two intrusion–extrusion runs (Run I and Run II) were then performed. The samples were evacuated for 2 h in a dilatometer placed in the Macropores Unit 120.

2.5.5. Scanning electron microscopy (SEM)

The morphology of the internal structure of the fabricated tablets with the highest (250 μm) and lowest (50 μm) values of the laser hatching distance was analysed with the SEM, as these tablets were expected to show the greatest differences in terms of the degree of fusion of the powder particles and the porosity achieved. The samples were coated with a gold alloy at 30 mA for 100 s on the BAL-TEC SCD 005 sputter coater (Leica Microsystems, Wetzlar, Germany) to improve their conductivity during imaging. Micrographs were taken using the JEOL JSM–6390LV scanning electron microscope (JEOL, Tokyo, Japan) at appropriate magnifications.

2.5.6. Tablet hardness

The breaking force of the tablets ($n = 10$) was measured with the ERWEKA TBH 125D hardness tester (ERWEKA, Langen, Germany) and the tensile strength was calculated according to Eq. (5):

$$\sigma = 2F/\pi Dt \quad (5)$$

where σ = tensile strength, F = breaking force, D = diameter and t = thickness of the tablet.

2.6. Drug assay

The tablets were crushed using a mortar and pestle ($n = 3$). The mass of each sample, which corresponded to the average mass of the tablet, was weighed and dissolved in a volumetric flask containing 10 mL methanol and shaken in an ultrasonic bath for 20 min. The samples were cooled to room temperature and then filtered through technical filter paper (FilterLab, Filtros Anoia, SA, Spain) and centrifuged at 5000 × g for 15 min. The amount of dissolved drug was determined by UV–VIS spectrophotometry (Evolution 300, Thermo Fisher Scientific, Waltham, MA, USA) at a wavelength of 238 nm, using placebo as a blank to exclude any interference. The calibration curve method with the required dilutions of the samples was used to calculate the ZT amount,

expressed as a percentage of the theoretical value with the standard deviation (SD). The measurements were performed in triplicate.

2.7. Disintegration of the tablets

The disintegration time of the tablets was measured in a compendial ERWEKA ZT 52 disintegration time tester (Erweka GmbH, Langen, Germany) with 800 mL distilled water as medium at 37 ± 0.5 °C. One tablet was placed in each of the six tubes of the basket and covered with a disc. The measurements were carried out in duplicate with six tablets per measurement.

2.8. In vitro drug release testing

The dissolution profiles of the tablets were determined using the USP-I Erweka DT 600 (Erweka, Langen, Germany) device. According to the Biopharmaceutical Classification System (BCS), ZT belongs to BCS class I and it has been reported in the literature that its solubility is not affected by pH values ranging from 1.2 to 6.8 (Paraiso et al., 2020). Therefore, distilled water was chosen as the medium for the dissolution test. The tablets of each formulation (n = 3) were placed in cylindrical baskets and immersed in 500 mL of distilled water for 4 h until the plateau was reached. The basket speed was set to 100 rpm and the tests were performed at 37 ± 0.5 °C. Aliquots (4 mL) were withdrawn at time intervals of 15, 30, 45, 60, 120, 180 and 240 min and filtered through 0.45 μm filters (Lab Logistics Group GmbH, Meckenheim, Germany). The amount of ZT released from the tablets was determined by UV–VIS spectrophotometry at 238 nm. The measurements were carried out in triplicate.

2.9. Differential scanning calorimetry (DSC) and X-ray powder diffraction (XRPD)

The DSC analysis was performed together with XRPD to analyse the physical state of the drug before and after the printing process. DSC measurements were performed using a DSC 1 instrument (Mettler Toledo, Giessen, Germany). Accurately weighed samples (4–7 mg) were placed in perforated aluminium dishes and heated at 10 °C/min in the range of 25 to 360 °C with a constant nitrogen gas flow of 50 mL/min, using an empty aluminium dish as a reference. The data obtained were analysed using STARe software (version 12.10, Mettler, Toledo), while XRPD measurements were performed on an Empyrean analytical powder diffractometer, Malvern P, at room temperature using Ni-filtered Cu Kα 1.2 radiation, scintillation detector and Bragg-Brentano focusing geometry. The applied intensity and voltage were 45 kV and 40 mA. The XRPD patterns were recorded in an angular range of 4–70° 2θ with a step size of 0.003° at a rate of 58 s per step.

2.10. Fourier-transform infrared spectroscopy (FTIR)

FTIR spectroscopy was used to analyse possible interactions between the drug and the excipients used in the study. Spectroscopic analyses of the pure materials as reference and the thoroughly powdered tablets were performed using a Nicolet iS10 (Thermo Scientific, Waltham, MA, USA) FTIR spectrometer equipped with a single reflectance ATR system (Smart iTR, Thermo Scientific, Waltham, MA, USA) with diamond plate and ZnSe lens. The spectra were recorded in the frequency range from 4000 to 650 cm^{-1}, with a resolution of 2 cm^{-1}.

3. Results and discussion

3.1. Characterisation of pharmaceutical powder blend

3.1.1. Particle size distribution

In the PBF-LB process, the layer height should be predefined as one of the process parameters based on the properties of the powder blend. Particular attention should be paid to the particle size in order to achieve a uniform distribution of an active substance within the manufactured dosage forms as well as a smooth surface and suitable mechanical properties (Charoo et al., 2020; Wu et al., 2022; Tonello et al., 2023). To determine the appropriate layer thickness, the PSD of the prepared F603 powder blend was analysed and characterised by the diameters of the particles at the 10th, 50th and 90th percentile of the mass distributions, where d_{10} = 15.736 μm, d_{50} = 77.948 μm and d_{90} = 927.092 μm, respectively. The results obtained (Fig. 2) show that the F603 powder blend had a bimodal particle distribution, with most of the particles being smaller than 100 μm and only a small proportion of the particles being larger.

Based on the results obtained, the layer height was left at 100 μm, a default value given by the software. It is also reported in the literature that a particle size distribution of 40–100 μm is most suitable for PBF-LB printing (Wu et al., 2022). If the particle size is too large, the powder has a granular structure. Due to the difference in particle size (gradient effect), the segregation process is more pronounced and the roughness increases during the powder distribution process, while the precision and surface finish of the part are reduced. On the other hand, the powder with a small particle size tends to stick to the roller due to the electrostatic effect, which also affects the powder distribution process. In addition, small particles can be harmful to the 3D printer itself, as they can penetrate the internal parts of the machine and cause damage (Gueche et al., 2021; Wu et al., 2022). Therefore, the prepared F603 powder blend was additionally sieved through a 125 μm sieve before the 3D printing to break up large particle aggregates that had formed due to the effect of cohesive forces during the mixing process and to ensure sufficient homogeneity of the powder blend while improving the smoothness of the tablet surface and avoiding subsequent variations in the uniformity of dosage units.

3.1.2. Powder flow properties

In addition to the particle size distribution, the flowability and bulk density of the powders are usually also considered as parameters that determine the effectiveness of the PBF-LB process itself. It has been described in the literature that poor flow properties of the powder blend and low bulk density lead to poor processing behaviour, especially when considering the spreading phase of the powder when fabricating a new layer (Lexow and Drummer 2016). Since the flowability of the particles, which is directly related to their size and distribution, is considered one of the critical properties of the powder feedstock for the PBF-LB process

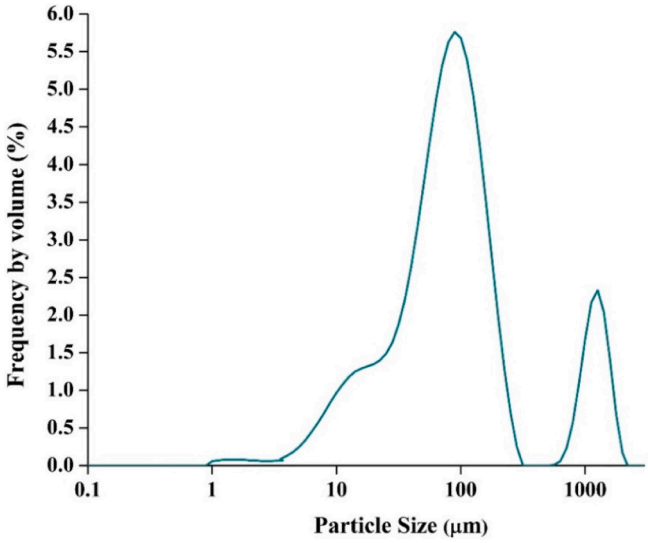

Fig. 2. Particle size distribution (PSD) of the pharmaceutical powder blend measured with laser diffraction and dry dispersion system.

(Thakkar et al., 2021), it was determined and the results are shown in Table 3. Based on the values of the compressibility index and the Hausner ratio, the prepared F603 powder blend exhibited passable flow properties. In general, powders with a Hausner ratio of less than 1.25 are considered free-flowing (Coe and Pasebani 2020). Given the results of the PSD analysis, the passable flow properties of the F603 powder blend are justified as particles with bimodal distribution types tend not to flow as freely as particles with narrower distribution types (Farzadfar et al., 2020). However, in terms of the powder bed fusion process, the low flowability could be overcome by adding a small amount of colloidal silica to the powder blends (Lexow and Drummer 2016; Levine et al., 2022). It has also been reported in the literature that powder blends with passable flow properties have been successfully used for 3D printing of pharmaceuticals (Madžarević et al., 2021).

3.2. 3D printing

The fabrication of the tablets was successfully carried out with different laser hatching distances, resulting in five different types of tablet formulations (Table 2). The use of low viscosity HPMC polymers for PBF-LB has already been described in the literature (Fina et al., 2018a; Madžarević et al., 2021). Fina et al. (2018a) have also shown that HPMC-based tablets with adequate mechanical properties can be successfully fabricated at different laser scanning speeds. However, in this study, the scanning speed was kept constant while the laser hatching distance was varied in a range from 50 to 250 μm. The surface temperature, which indicates the temperature of the powder in the build chamber during the printing process, was set at 150 °C, which is about 15 °C below the glass transition temperature (onset: 165.16 °C; midpoint: 171.43 °C) determined by DSC analysis for the PHARMACOAT® 603 polymer used in this study. The difference between the surface temperature and the chamber temperature was kept at 20 °C, which was also indicated in the literature as the optimum difference between these two temperatures during the 3D printing (Fina et al., 2017; Trenfield et al., 2022). Once again, the suitability of HPMC as a polymer for the PBF-LB process was confirmed, even when the distance between two successive laser beams was varied. As with the other excipients, Candurin® Gold Sheen, a golden pearlescent pigment commonly used in tablet coatings, was added to the formulation to improve printability. 3 % (w/w) of this pigment has been shown to be optimal for the PBF-LB process (Fina et al., 2017), so the same amount was used in the present study. The flowability of the powder blend was improved by adding a small amount of colloidal silicon dioxide (0.5 % w/w).

In the PBF-LB process, the degree of powder fusion is determined by several parameters, but above all by the energy density, i.e. the amount of energy transferred per unit volume. This critical parameter depends on four process parameters, as shown in Eq. (6):

$$ED = \frac{LP}{SS \times HD \times LT} \tag{6}$$

where ED = energy density, LP = laser power, SS = scanning speed, HD = hatching distance and LT = layer thickness (Beitz et al., 2019).

Based on the results obtained, it was found that the hue of the yellow colour of the tablets produced becomes lighter with increasing laser hatching distance, while the other process parameters were kept constant (Fig. 3).

The obtained results may be explained by the fact that the lower energy per unit volume of the powder blend was transferred, which consequently also led to a lower powder fusion effect (Shirazi et al., 2015). This confirms that the laser hatching distance as a process parameter significantly influences the energy density and the powder bed fusion process itself. Similar results were obtained in the study by Trenfield et al. (2022), but instead of the laser hatching distance, the laser scanning speed, as one of the process parameters that also influences energy density, was varied. Regarding the build cycle, it has been reported in the literature that the laser hatching distance is directly proportional to the fabrication speed (Kumar, 2014). At larger distances, the laser takes less time to scan the layer, whereas at a small distance, multiple scans are required to process the entire layer, which takes more time (Kumar, 2014). In line with this data, the time required for a manufacturing lot of six tablets depended on the system set-up for each formulation, i.e. the value of the laser hatching distance, which was varied, and ranged from 17 min (F603 250) to 29 min (F603 50).

Table 3
The flowability of the pharmaceutical powder blend.

Formulation	Direct flowability ($g\ s^{-1}$ ± SD)	Compressibility index (% ± SD)	Hausner ratio
F603	2.16 ± 0.05	21.74 ± 3.86	1.28 ± 0.06

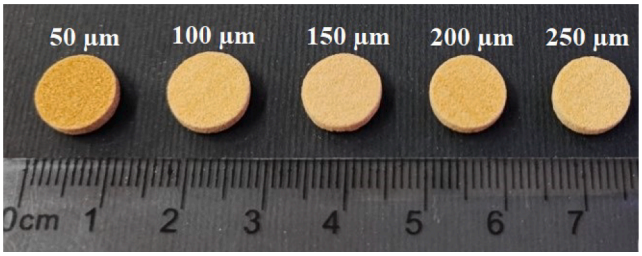

Fig. 3. Images of tablets fabricated with increasing laser hatching distance (from left to right). The scale is in cm.

3.3. Physical and mechanical characteristics of the tablets

3.3.1. Tablet morphology, weight and density

The tablets obtained were yellow due to the added pigment, with a characteristic layered structure and a uniform cylindrical shape as-designed. As explained in the section above (3.2 3D Printing), the colour intensity decreased with increasing laser hatching distance, which is clearly visible in the tablets fabricated with the highest (250 μm) and lowest value of this process parameter (50 μm) (Fig. 3). The physical and mechanical properties of the tablets are listed in Table 4. In general, the results obtained show that lower laser hatching distances correlate with higher tablet weight and density than higher laser hatching distances. While, as expected, the most significant difference in tablet weight and density is observed between the tablets with the highest (F603 250) and lowest (F603 50) values of this process parameter. In the literature, the influence of the laser hatching distance on the microstructure of the manufactured parts is explained by the overlap theory. The overlap refers to the extent to which a new laser line scans the previously scanned track. Thus, as the laser hatching distance is reduced, the scan lines move closer together until they overlap, improving the connection between the lines and reducing porosity (Shirazi et al., 2015; Padmakumar 2020). Based on this theory, denser tablets fabricated with smaller laser hatching distance are expected and vice versa. Trenfield et al. (2022) investigated the effect of laser scanning speed on the physical properties of tablets and found a strong linear correlation between laser scanning speed and tablet density (R^2 = 0.9883). In this study, a linear correlation was found between the values

Table 4
Physical and mechanical properties of the tablets.

Formulation	Diameter (mm ± SD)	Thickness (mm ± SD)	Weight (mg ± SD)	Tensile strength (MPa ± SD)
F603 50	9.93 ± 0.07	3.27 ± 0.08	218.35 ± 15.46	4.18 ± 1.02
F603 100	9.86 ± 0.06	3.26 ± 0.04	165.07 ± 3.43	1.45 ± 0.14
F603 150	9.94 ± 0.09	3.22 ± 0.07	148.81 ± 7.71	1.10 ± 0.14
F603 200	9.95 ± 0.04	3.18 ± 0.04	140.75 ± 7.84	1.04 ± 0.29
F603 250	9.96 ± 0.13	3.16 ± 0.02	135.50 ± 4.70	0.59 ± 0.08

of the laser hatching distance in the range of 100 – 250 μm and the tablet density (R^2 = 0.9391, Fig. 4b). However, the tablet density at a laser hatching distance of 50 μm does not follow the linear trend (R^2 = 0.7991, Fig. 4a). It can be concluded from the results that the tablet density is predictable at higher values of laser hatching distance. 93.91 % of the variance in tablet density is predicted by the laser hatching distance value for the F603 tablet formulation. However, a strong linear correlation was not found when all levels of variation in laser hatching distance were considered, which raises a new question for further investigation.

3.3.2. *Mercury intrusion porosimetry (MIP)*

The MIP measurements, which include total pore volume, specific surface area, average pore diameter, bulk density and porosity of the fabricated tablets (n = 3), are listed in Table 5. In order to define the nature of porosity more precisely, the analysis was performed in two consecutive cycles of mercury intrusion. During the first Hg intrusion cycle, the mercury filled both the interparticle (voids) and intraparticle spaces, while in the second measurement cycle, the mercury could only occupy the space of accessible pores (intraparticle space) (Tanaka and Sakai, 2023). Based on the results obtained, the difference between the first and second cycle when considering the two end points of the laser hatching distance (50 μm and 250 μm) was significantly greater for the tablets fabricated with a higher value of this process parameter. However, as inter-particle porosity is a characteristic of mostly powder samples, in this case, where the tablets fabricated by PBF-LB were analysed, the type and shape of the pores are responsible for the discharge and availability during the repeated cycles of mercury intrusion. The samples have a low porosity, ranging between 10 and 18 % in the first cycle and between 5 and 9 % in the second cycle.

The integral and differential curves shown in Fig. 5 illustrate the multimodal character of the tablet samples. They show the presence of pores of different sizes, from mesopores (10–20 nm) in the tablets fabricated with a laser hatching distance of 50 μm, 200 μm and 250 μm (Fig. 5a, 5d and 5e), to macropores (>50 nm) in the tablets fabricated with a laser hatching distance of 100 μm and 150 μm (Fig. 5b and 5c).

In accordance with the theory on the influence of the laser hatching distance on the mechanical properties of the fabricated parts (Shirazi et al., 2015; Padmakumar 2020) and based on the results of the porosimetric measurements for the tablets obtained in this study, it is assumed that at lower values of the laser hatching distance, the successful formation of stable pores occurs due to the successful bonding of the powder particles during the powder fusion process itself. Under the influence of the laser beam, a sufficient amount of energy was applied to fuse the particles and successfully form a stable system of voids and channels with solid walls, enabling the fabrication of tablets with low porosity (Table 5). This is evident from the low percentage decrease in porosity (30.8 %) in the second intrusion cycle for the tablets fabricated with a laser hatching distance of 50 μm. The decrease in porosity in the second intrusion cycle indicates the presence of a specific type of pores, classified as ink-bottle pores when studying the porous structure of materials, which are difficult to unload due to their specific structure and remain inaccessible in the next intrusion cycle (Zhang et al., 2022). This is reflected in the decrease in total pore volume shown in Table 5. The hardness of over 2 MPa determined for the F603 50 tablets may also indirectly indicate the formation of solid walls between the cavities, i.e. a higher force had to be applied when testing the breaking strength of the tablets (Table 4). In contrast, the decrease in porosity in the second cycle of mercury intrusion (61.8 %) is more pronounced in the tablets fabricated with the highest laser hatching distance (250 μm). In this case, the voids between the particles are more pronounced, and due to the lower energy input during the PBF-LB process, a lower degree of fusion between the powder particles was achieved, so that the resulting tablets also exhibited significantly poorer mechanical properties (Table 4).

The porosity of SLS 3D-printed dosage forms has also been investigated in more detail in the literature using micro-computed tomography (micro-CT). Kulinowski et al. (2021) have shown that printing paracetamol-loaded printlets with denser hatch spacing results in the

Table 5
MIP measurements on the fabricated tablets (F603 50–F603 250).

Formulation	Run	[1]V_{tot} ($mm^3\ g^{-1}$)	[2]S_{Hg} ($m^2\ g^{-1}$)	[3]D_{av} (nm)	[4]BD ($g\ cm^{-3}$)	[5]P (%)
F603 50	I	109.04	17.98	20	1.18	12.86
	II	75.46	21.84	8	1.18	8.90
F603 100	I	158.45	11.98	9784	1.14	18.06
	II	23.67	3.79	10	1.14	2.69
F603 150	I	87.22	8.73	9784	1.25	10.90
	II	41.32	7.44	12	1.25	5.16
F603 200	I	92.82	9.86	80	1.24	11.51
	II	62.58	8.20	20	1.24	7.76
F603 250	I	108.63	12.17	10	1.23	13.36
	II	41.53	8.43	8	1.23	5.10

[1] Total pore volume.
[2] Specific surface area.
[3] Pore diameter average.
[4] Bulk density.
[5] Porosity.

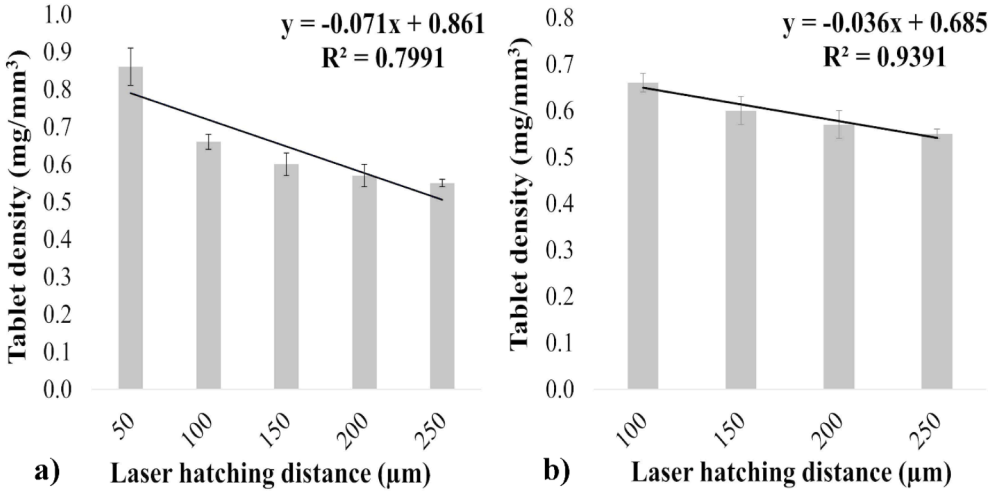

Fig. 4. Average calculated density of tablets fabricated with: a) laser hatching distances in the range between 50 – 250 μm and b) laser hatching distances in the range between 100 – 250 μm, with decreasing tendency.

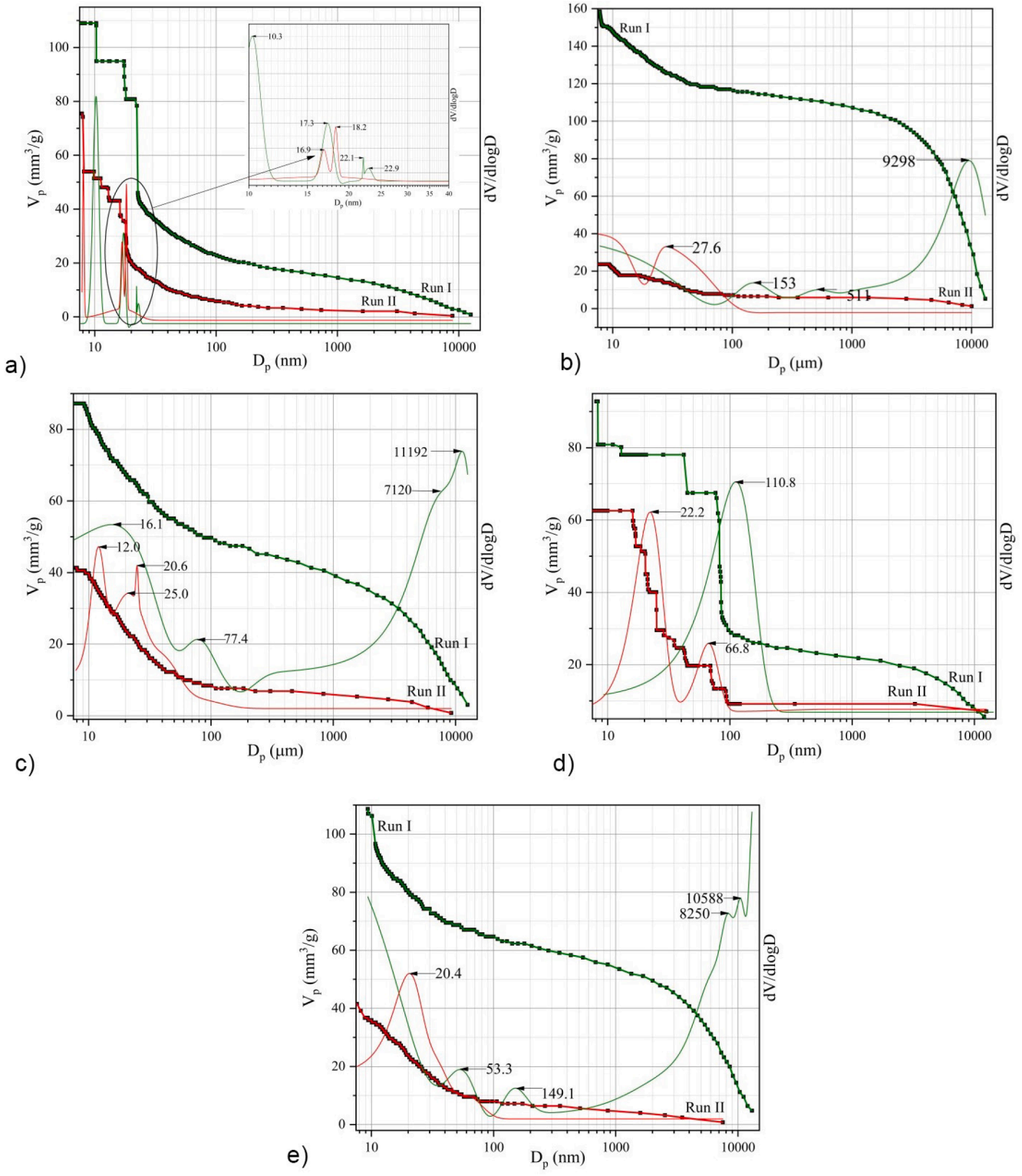

Fig. 5. Pore size distribution curves for the tablets fabricated with increasing laser hatching distances: a) F603 50, b) F603 100, c) F603 150, d) F603 200 and e) F603 250.

porosity of the printlets decreasing from the bottom to the top of the matrix, while the topology of the pore space shows the formation of a continuous network within the printlets. Fewer filaments were formed in the printlets fabricated with smaller hatch spacings, while increasing the hatch spacing led to a broadening of the pore thickness distribution towards higher values (Kulinowski et al., 2021). On the other hand, in a more recent study, Tabriz et al. (2023) also investigated the effect of different laser powers on the micro- and macroporosity of personalised carvedilol dosage forms. The printlets fabricated with less intense laser power exhibited slightly greater macroporosity, while microporosity remained unchanged, suggesting that macroporosity determines laser power-dependent porosity (Tabriz et al., 2023). The MIP results obtained in this study are in good agreement with the results published in the literature. It is expected that in the upper layer of tablets fabricated

with denser hatch spacing, the pore channels disappear due to the higher melting degree of the powder, which is also consistent with the overlap theory of laser line scanning (Shirazi et al., 2015; Padmakumar 2020; Kulinowski et al., 2021). However, it should be noted that further investigation would be beneficial for a thorough analysis of the walls of the channels and pores within the printed tablets.

3.3.3. Scanning electron microscopy (SEM)

The SEM images of the internal structure of the tablets provided visual confirmation of the porosity and grain growth in both samples of the tablets (Fig. 6).

Based on the results obtained, it can be seen that the tablets fabricated with a higher laser hatching distance of 250 μm show a partial fusion of the powder particles with irregularly shaped pores (Fig. 6a). Compared to the internal structure of the tablets fabricated with a smaller laser hatching distance of 50 μm, the bridges between the particles were firmly solidified and the pores were closed in a regular spherical shape (Fig. 6b). Similar results were obtained by Kulinowski et al. (2021), where a smaller laser hatching distance led to a change in the internal structure of the fabricated paracetamol dosage forms, resulting in a strong intermixing of the neighbouring grains and the solidification of large complex particles with a smoother surface. The results obtained confirm that a reduction in the laser hatching distance leads to a higher degree of fusion of the powder, resulting in fewer voids between the individual particles and thus a denser internal structure of the tablets. Therefore, better mechanical properties with a prolonged disintegration time and a prolonged dissolution rate of the drug were achieved. However, both tablet samples exhibit areas of free powder particles caused by the partial powder fusion mechanism, i.e. a small amount of free powder remains trapped in the porous structure of the layers during the 3D printing process itself (Allahham et al., 2020; Madžarević et al., 2021).

3.3.4. Tablet hardness

Laser hatching distance was also found to affect the tensile strength of the tablets, with tablets fabricated with lower laser hatching distances having higher tensile strength values than tablets fabricated with higher values for this process parameter (Table 4). It is reported in the literature that a minimum strength of 2 MPa is required to ensure tablet integrity under normal handling and that this is a generally accepted empirical criterion for the tabletability of conventional tablets (Sun et al., 2009; Osei-Yeboah and Sun 2015). The influence of PBF-LB process parameters on tablet hardness has been investigated and it has been found that higher temperatures and lower values of laser scanning speed result in more compact tablets (Fina et al., 2018a; Barakh Ali et al., 2019; Mohamed et al., 2020; Trenfield et al., 2022). The acceptance criterion for the tensile strength of 3D-printed tablets has not yet been defined, as PBF-LB technology has only recently been used in the pharmaceutical sector. However, it is not justified to set the limit values for the tensile strength of 3D printed dosage forms so high and to expect that these tablets must necessarily fulfil the general criteria for the mechanical properties of compact tablets. The internal structure of 3D-printed tablets is quite different due to the sintering effect, i.e. the powder fusion mechanism, and also differs significantly from compact tablets due to the layering mechanism (Fina et al., 2018a; Tabriz et al., 2023). Despite the lack of some general criteria in the state of the art, it was found that even the tablets fabricated with higher values of laser hatching distance had acceptable mechanical properties in terms of handling and storage, i.e. withstood the stress conditions during the research process itself. While the tablets fabricated with the laser hatching distance of 50 μm even met the generally recognised criterion for tabletability with an average tensile strength of 4.18 ± 1.02 MPa. To summarise, in order to fabricate tablets with a denser structure and consequently a higher tensile strength, it is of utmost importance to adjust not only the temperature and speed of the laser, but also the laser hatching distance. As

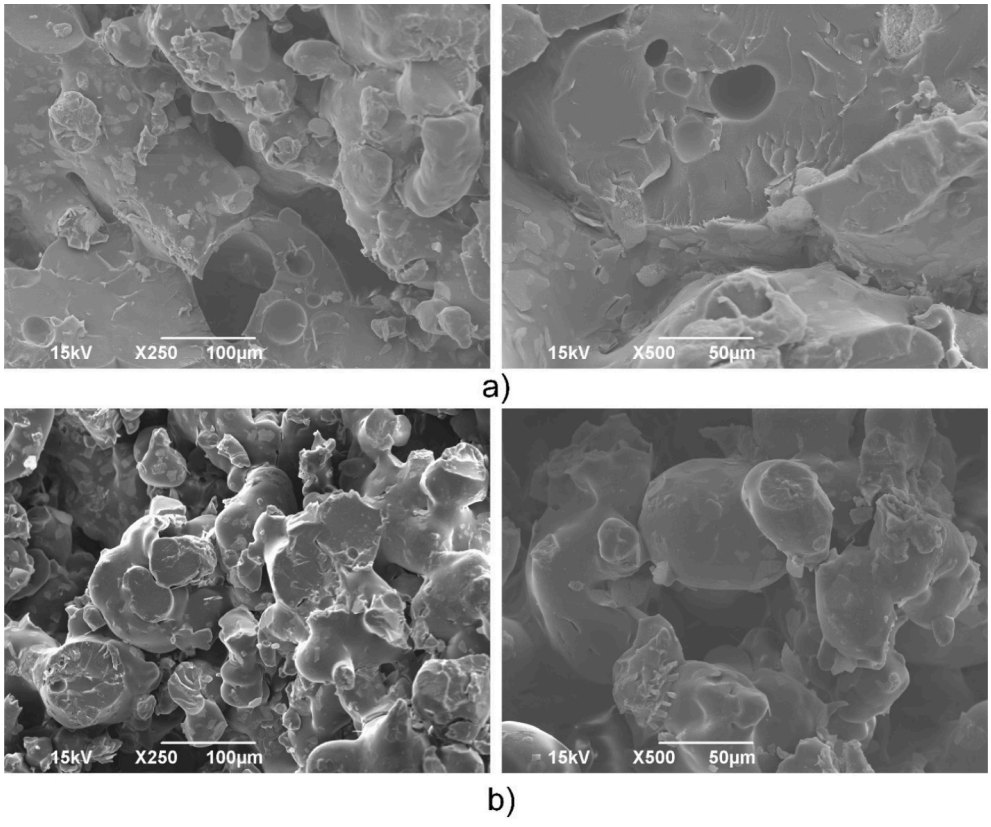

Fig. 6. SEM images of the internal structure of the fabricated tablets with the laser hatching distances: a) 50 μm and b) 250 μm, at different magnifications (×250 on the left and × 500 on the right).

this process parameter has a significant influence on the mechanical properties of the PBF-LB tablets.

However, it should be noted that printed PBF-LB tablets would require a different type of packaging than conventional push-through blisters due to their generally poorer mechanical properties (Fina et al., 2018a). Providing clear instructions to patients on how to handle this type of tablet could be a possible solution to overcome the problem of poor mechanical properties. This is also supported by the general idea of 3D printing of medicines to provide patients with small batches of drugs specifically tailored to their needs (Allahham et al., 2020). Nevertheless, it is worth mentioning that recently it has been reported in the literature that printed medicines as innovative dosage forms also require changes in the methodology for their evaluation (Seoane-Viaño et al., 2023), implying the fact that new criteria should also be considered when evaluating the properties of 3D printed dosage forms.

3.4. Drug assay

The drug assay showed that no degradation of the active substance had occurred during the 3D printing, even though high powder bed temperature was used. The values obtained were within 90–110 % of the theoretical amount of the active substance (Table 6), which is consistent with the acceptable limits of the United States Pharmacopoeia monograph for conventional zolpidem tartrate tablets (The United States Pharmacopeia, 2021).

Based on the amount of ZT determined in the tablets fabricated with different laser hatching distances, it can be seen that this process parameter influences the amount of an active substance contained. For example, tablets fabricated with a laser hatching distance of 50 μm would provide a dose of 11.53 mg ZT compared to 6.65 mg ZT for tablets fabricated with a laser hatching distance of 250 μm, and with the same dimensions (Table 6). The importance of laser scanning speed and temperature during PBF-LB printing and their influence on the formulated dose have already been described in the literature (Mohamed et al., 2019; Trenfield et al., 2022), while the influence of laser hatching distance has, to the best of our knowledge, not yet been investigated in relation to dosage tailoring. Therefore, great attention should be paid to all PBF-LB process parameters in terms of their impact on 3D printing of dosage forms with the desired dose. To better understand the influence of this process parameter on ZT dosage, a linear correlation between the amount of ZT incorporated into the tablets and the laser hatching distance was estimated. It was found that approximately 75 % of the variance in the amount of ZT could be predicted by the laser hatching distance ($R^2 = 0.7389$, Fig. 7).

However, the results obtained relate only to a single formulation containing 5 % (w/w) of the active substance. Therefore, further studies are needed to confirm and clarify the degree of correlation between the amount of active substance incorporated into the fabricated dosage forms and the laser hatching distance used. Nevertheless, the approach of varying only one process parameter while obtaining tablets with a wider dosage range could be used as an important tool for printing dosage forms with precise dose. In view of the fact that the laser hatching distance not only has a significant influence on the drug content, but also on the physical and mechanical properties of the manufactured tablets themselves, the PBF-LB process could play an important role in the individualisation of the therapy through process parameters. With regard to ZT dose tailoring, this could be of particular importance if a gradual withdrawal of the drug from therapy is required and therefore a gradual dose reduction is necessary (Henry et al., 2021). Instead of using standard techniques such as tablet splitting with already established dosages on the market, which have proven to be quite unreliable (Tikhomirov, 2023), the production of 3D-printed dosage forms with precise ZT dosing could be a possible solution to support the development of a flexible dosing platform.

Table 6
Drug assay expressed as the amount of ZT contained in the tablets (mg ± SD) and as a percentage of the theoretical value (% ± SD).

Formulation	Drug assay	
	(mg ± SD)	(% ± SD)
F603 50	11.53 ± 0.11	105.65 ± 1.03
F603 100	8.24 ± 0.08	99.81 ± 0.94
F603 150	6.94 ± 0.02	93.30 ± 0.26
F603 200	6.92 ± 0.11	98.35 ± 1.50
F603 250	6.65 ± 0.25	98.44 ± 2.74

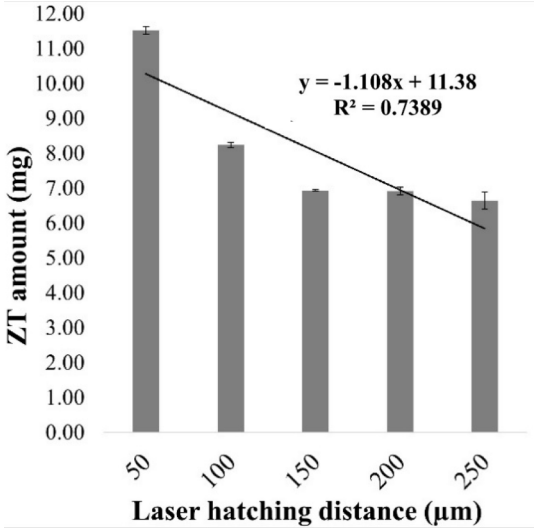

Fig. 7. Average amount of incorporated ZT in tablets fabricated with different laser hatching distances with decreasing tendency.

3.5. Disintegration of the tablets

The time required for the disintegration of the tablets varied between 22.73 ± 0.21 min (laser hatching distance 250 μm) and 72.02 ± 7.19 min (laser hatching distance 50 μm) (Fig. 8).

The disintegration time of tablets fabricated with higher laser hatching distances (100–250 μm) showed a decreasing tendency, but

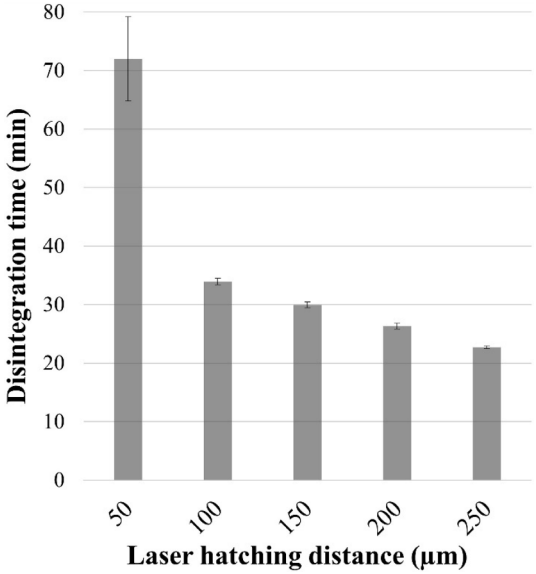

Fig. 8. Effect of increasing laser hatching distances on the disintegration time of tablets.

with quite similar values around 30 min. Madžarević et al. (2021) also reported similar disintegration test results when tablets were fabricated from low molecular weight HPMC with higher energy density input. However, tablets fabricated with a laser hatching distance of 50 μm took twice as long to disintegrate as tablets fabricated with a higher laser hatching distances, suggesting that a slower release of the drug can be achieved. The decrease in disintegration time with the increase in laser hatching distance could be explained by the lower energy input, which allows the powder particles in the tablet to separate from each other as soon as they come into contact with the dissolution medium (Fina et al., 2018a; Madžarević et al., 2021). As explained in the section above (3.2 3D Printing), the energy density is inversely proportional to the laser hatching distance. Therefore, tablets fabricated with higher values of this process parameter are expected to disintegrate faster than tablets fabricated with lower values, as the powder bed fusion process had been carried out with lower energy input. A lower degree of overlap between two consecutive laser lines during 3D printing leads to a lower degree of fusion of the polymer and the formation of liquid–solid bridges between the powder particles and thus to a less dense tablet structure (Olakanmi et al., 2015; Kulinowski et al., 2021). This allows the medium to penetrate the pores more easily and break the brittle bonds between the particles more quickly, which accelerates the disintegration process, which is also consistent with the results of the MIP and SEM analyses.

3.6. *In vitro drug release testing*

Using the basket apparatus, all tablets were tested for 4 h for their drug release in distilled water. It was found that the release rate of ZT increased as a function of a laser hatching distance (Fig. 9).

Similar dissolution test results were reported by Trenfield et al. (2022) when the release rate of theophylline was investigated as a function of laser scanning speed, and a decreasing trend was observed between the release profiles obtained with decreasing laser scanning speed. However, in this study, the most significant decrease in drug release over time was observed in tablets fabricated with the lowest value of laser hatching distance, while the differences in drug release were not significantly pronounced in tablets fabricated with higher values of this process parameter. For example, tablets fabricated with lower laser hatching distances (F603 100–F603 250) released about 70 % of the ZT within 45 min, while tablets fabricated with a laser hatching distance of 50 μm (F603 50) released about 45 % of the drug in the same time, which is also in good agreement with the results obtained for tablet disintegration. The decrease in drug release in tablets fabricated with increasing energy input can be explained by its influence on the physical properties of the tablets. Higher values of the laser hatching distance led to a less dense and more porous tablet structure, which allows easier penetration of the medium and thus a faster dissolution rate of the drug (Kulinowski et al., 2021).

According to the recommendations for dissolution testing in the European Pharmacopoeia, edition 11.0, the acceptance criterion for S1 conventional release dosage forms is that at least 80 % of the active substance is released within a specified time, usually 45 min or less, whereas the acceptance criterion for prolonged release dosage forms should normally consist of 3 or more points. The 1st specification point serves to prevent unintended rapid release of the active substance ('dose dumping') and the criterion corresponds to a dissolved amount of typically 20–30 %. The 2nd specification point defines the dissolution pattern and is therefore set at a release of about 50 %, while the last specification point is intended to ensure a near–complete release, which is generally understood as more than 80 % release. Taking into account the dissolution test criteria specified in the European Pharmacopoeia, tablets fabricated with lower laser hatching distances (F603 100–F603 250) are more likely to have an immediate release of the active substance, whereas tablets fabricated with a laser hatching distance of 50 μm (F603 50) exhibited a slower dissolution of the active substance, with 50 % of the dose being released within the first hour and the other half of the dose being released gradually. Compared to conventional tablets, which are usually produced by direct compression with the addition of disintegrating agents that cause the tablet to disintegrate in the gastrointestinal tract and release the active substance so that it can be dissolved and absorbed (Maclean et al, 2021). Tablets manufactured using the PBF-LB process as unconventional dosage forms are usually produced without disintegrating agents, while their layered and porous structure supports the disintegration process and allows the immediate release of the drug (Fina et al., 2018a; Barakh Ali et al., 2019; Allahham et al., 2020). However, depending on the degree of porosity, the type of pore system created and the strength of the bonds between the particles achieved by the process parameters, fabricated tablets can also combine the initial and maintenance dose in the same dosage form, which was achieved in this study. Despite the lack of regulatory criteria, the fact is

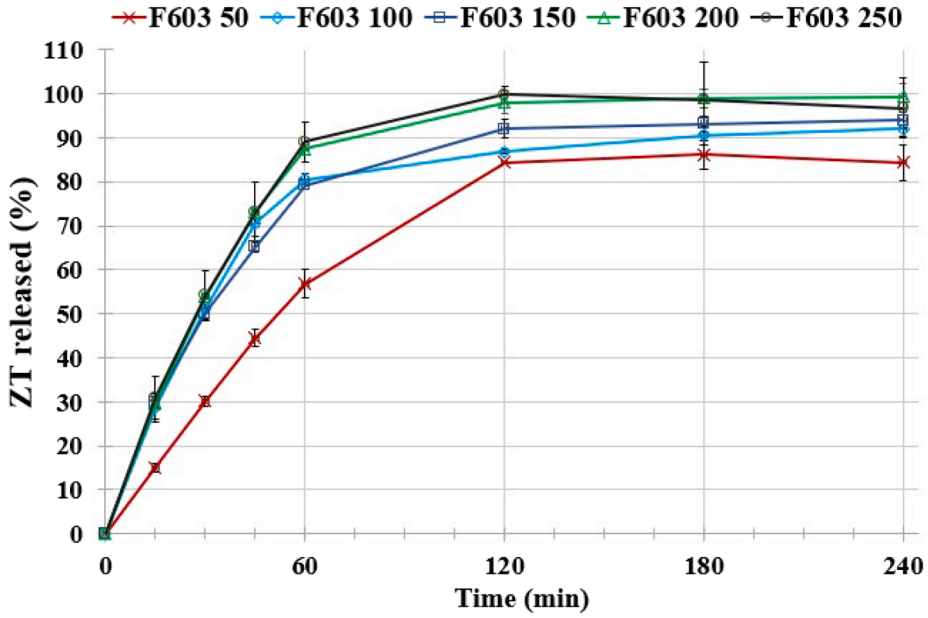

Fig. 9. Dissolution profiles of the fabricated tablets (F603 50–F603 250).

that these innovative dosage forms could provide customised drug release profiles achieved by different approaches (Tikhomirov et al., 2023). Nevertheless, further research is certainly needed, not only on process parameters and formulation factors, but recent studies also suggest that special attention should be paid to the methodology of disintegration and dissolution testing due to the unique characteristics of 3D printed formulations (Seoane-Viaño et al., 2023).

3.7. Differential scanning calorimetry (DSC) and X-ray powder diffraction (XRPD)

The crystalline state of the active substance and polymers in the F603 powder blend and fabricated tablets was analysed using XRPD and DSC. The DSC thermograms and XRPD diffractograms of the formulations containing ZT (5 % w/w) fabricated with different laser hatching distances (F603 50–250), the prepared powder blend (F603 powder blend), the pure polymer (HPMC) and the active substance (ZT) are shown in Fig. 10a and 10b, respectively.

The DSC thermogram of the F603 powder blend shows a small endothermic peak at about 120 °C, which coincides with the endothermic peak of the ZT, indicating a loss of water bound in the crystal lattice (Henry et al., 2021) (Fig. 10a). However, the sharp endothermic peaks at around 190 °C and 210 °C, corresponding to the free zolpidem base and zolpidem hydrogentartrate, respectively, were not detected in the thermogram of the F603 powder blend. This is possibly due to the small amount of active substance (Ettema et al., 2005; Fina et al., 2018a) and/or the dissolution of the active substance in the polymer due to the heating process during the analysis itself. All formulations tested, including the prepared powder blend, showed a broad endotherm before 100 °C, corresponding to water evaporation and polymer relaxation (Fina et al., 2018a; Tikhomirov et al., 2023). However, melting peaks corresponding to the free base of zolpidem or zolpidem hydrogen tartrate were not observed in any of the formulations, suggesting that the drug was either molecularly dispersed as a solid dispersion in the polymer matrix or that the drug self-dissolved in the polymer due to the elevated temperature during DSC analysis (Fina et al., 2018a; Trenfield et al., 2022). Nevertheless, a small amount of ZT in the tablets could also be the reason for the absence of the main peaks.

To further clarify and confirm the physical state of the drug, the XRPD diffractograms of the fabricated tablets were observed. It can be seen in Fig. 10b that the XRPD diffractograms are in good agreement with the observations from the thermograms and confirm the amorphous patterns in all the formulations. The most prominent ZT peak at 8.9° can be seen in the diffractogram of the F603 powder blend (Fig. 10b), although its intensity was significantly reduced due to the low amount of ZT. This result indicates the crystalline form of the active substance in the prepared powder blend before 3D printing, which cannot be observed in the fabricated tablets afterwards. The results obtained for all the tablet formulations produced clearly show that the ZT was in its amorphous state, suggesting that the change in physical state occurred during the 3D printing process itself. Amorphisation of the drug during the PBF-LB process has been reported in the literature (Fina et al., 2018a; Hamed et al., 2021; Madžarević et al., 2021; Tikhomirov et al., 2023). The influence of the directed laser beam on the powder surface and the increased temperature can lead to a reduction in the degree of crystallinity, which makes the physical state of the drug more favourable from the point of view of bioavailability. This finding could be of particular importance for formulations consisting of poorly soluble drugs, such as BCS class II or IV (Yu et al., 2018; Davis et al.,2021; Madžarević et al., 2021; Chatterjee et al., 2022).

3.8. Fourier-transform infrared spectroscopy (FTIR)

Fourier transform infrared spectroscopy (FTIR) was performed to investigate possible drug-polymer interactions. The FTIR spectra of the tablet formulations containing ZT (5 % w/w) fabricated with different laser hatching distances (F603 50–250), the prepared powder blend (F603 powder blend), the pure polymer (HPMC) and the active substance (ZT) are shown in Fig. 11.

The FTIR spectrum of HPMC showed a very broad absorption band of the hydroxyl group (OH) in the range of 3100–3600 cm^{-1}. The aliphatic CH stretching appeared at about 2900 cm^{-1}. The alcoholic C-O stretching was seen at 1100 cm^{-1}, while the aliphatic C-O band appeared at 1050 cm^{-1}. Similar FTIR results for low molecular weight HPMC were reported by Sadeghi et al. (2022). The main peak at around 1640 cm^{-1} identified in the pure ZT spectrum, corresponding to the strong absorption band of the carbonylamide (R_2NCO) stretch (Prajapati et al., 2011), was observed in the spectra of all tablet formulations at the same wavenumber, confirming the absence of significant interactions between the ZT and the excipients used.

4. Conclusion

PBF-LB as a newly applied 3D printing technology in the field of tablet manufacturing opens up a new perspective for the fabrication of medicines tailored to the individual needs of patients. This technology in combination with traditionally used excipients transforms known formulations into a completely new form of drug delivery whose internal

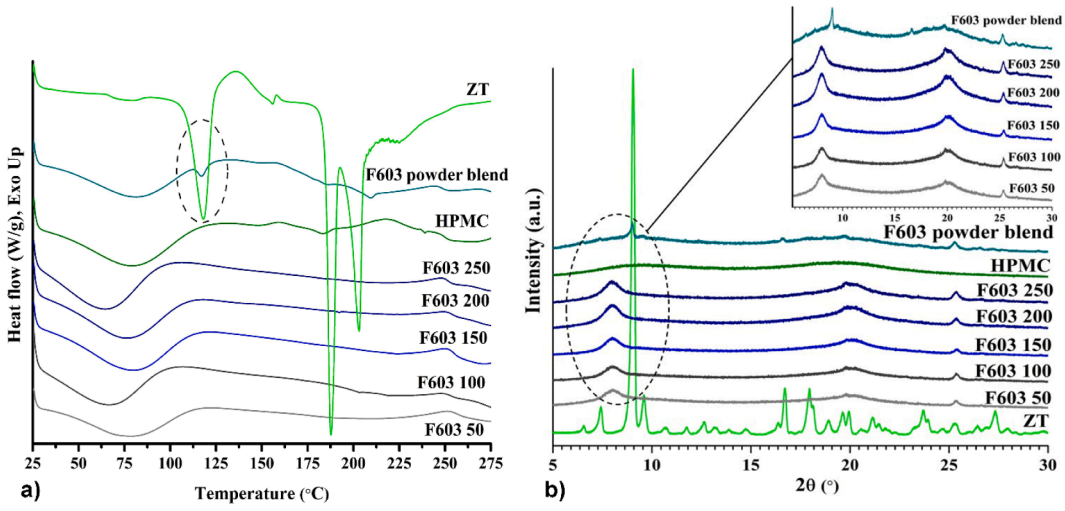

Fig. 10. Solid state characterisation of the formulations fabricated with different laser hatching distances (F603 50–250), the prepared powder blend (F603 powder blend), the pure polymer (HPMC) and the active substance (ZT): a) DSC thermograms and b) XRPD diffractograms.

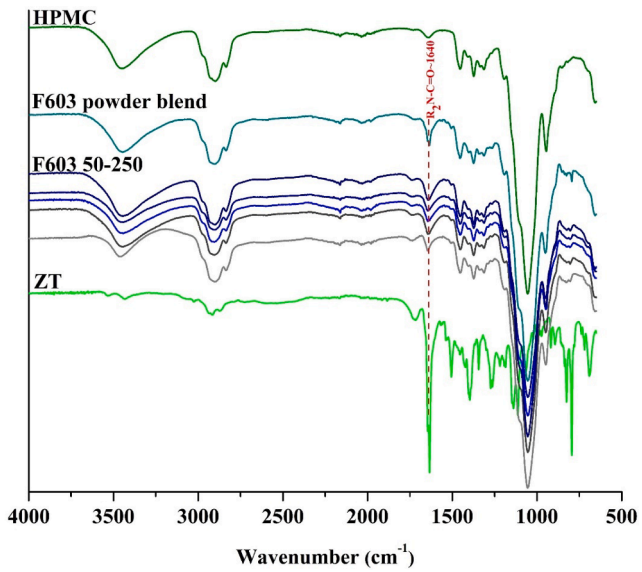

Fig. 11. FTIR spectra of the tablet formulations fabricated with different laser hatching distances (F603 50–250), the prepared powder blend (F603 powder blend), the pure polymer (HPMC) and the active substance (ZT).

structure, degree and type of porosity can be customised by varying numerous process parameters to achieve the desired dosages and release profiles. Therefore, it is of utmost importance to investigate and consider all process parameters of the PBF-LB process that could influence the in vitro behaviour of the manufactured dosage forms. The data obtained in this study indicate that laser hatching distance, as one of the process parameters that strongly influences the laser energy input and thus the properties of the fabricated dosage forms, plays an important role in obtaining tablets with suitable mechanical and physicochemical properties that provide unique drug dissolution profiles with tailored ZT dosages. And overall contribute to a better understanding of the PBF-LB process in the manufacture of dosage forms while highlighting the potential for therapy individualisation. However, despite the fact that valuable insights have been gained, there is still a lack of clear guidance for the selection of suitable process parameters without prior failed trials, which represents a new starting point for further research.

Funding

This work was supported by the Ministry of Science, Technological Development and Innovation of the Republic of Serbia through the Grant Agreement with the University of Belgrade – Faculty of Pharmacy No.: 451-03-65/2024-03/200161; 451-03-66/2024-03/200161.

CRediT authorship contribution statement

Ivana Adamov: Writing – original draft, Methodology, Investigation, Formal analysis, Data curation, Conceptualization. **Gordana Stanojević:** Writing – review & editing, Supervision, Methodology, Formal analysis, Data curation, Conceptualization. **Stefan M. Pavlović:** Methodology, Investigation, Formal analysis, Data curation. **Djordje Medarević:** Methodology, Investigation, Formal analysis. **Branka Ivković:** Methodology, Investigation. **David Kočović:** Methodology, Investigation. **Svetlana Ibrić:** Writing – review & editing, Supervision, Resources, Methodology, Investigation, Funding acquisition, Formal analysis, Data curation, Conceptualization.

Declaration of competing interest

The authors declare that they have no known competing financial interests or personal relationships that could have appeared to influence the work reported in this paper.

Data availability

Data will be made available on request.

Acknowledgements

The authors would particularly like to thank Mr Samir Nasser-Eddin Vélez and HARKE Pharma GmbH (Mülheim, Germany) and Shin-Etsu Chemical Co, Ltd (Tokyo, Japan) for their kindness and generosity in providing the excipients used in this study and Professor Vladimir Pavlović for SEM analysis.

References

Abdalla, Y., Elbadawi, M., Ji, M., et al., 2023. Machine learning using multi-modal data predicts the production of selective laser sintered 3D printed drug products. Int. J. Pharm. 633, 122628 https://doi.org/10.1016/j.ijpharm.2023.122628.

Adamov, I., Stanojević, G., Medarević, D., et al., 2022. Formulation and characterization of immediate-release oral dosage forms with zolpidem tartrate fabricated by digital light processing (DLP) 3D printing technique. Int. J. Pharm. 624, 122046 https://doi.org/10.1016/j.ijpharm.2022.122046.

Allahham, N., Fina, F., Marcuta, C., et al., 2020. Selective laser sintering 3D printing of orally disintegrating printlets containing ondansetron. Pharmaceutics 12 (2), 110. https://doi.org/10.3390/pharmaceutics12020110.

Spritam. Aprecia Pharmaceuticals, USA. Accessed January 9, 2024. Available from: https://www.spritam.com/#/patient.

Awad, A., Fina, F., Trenfield, S.J., et al., 2019. 3D printed pellets (Miniprintlets): A novel, multi-drug, controlled release platform technology. Pharmaceutics 11 (4), 148. https://doi.org/10.3390/pharmaceutics11040148.

Awad, A., Fina, F., Goyanes, A., Gaisford, S., Basit, A.W., 2020. 3D printing: Principles and pharmaceutical applications of selective laser sintering. Int. J. Pharm. 586, 119594 https://doi.org/10.1016/j.ijpharm.2020.119594.

Barakh Ali, S.F., Mohamed, E.M., Ozkan, T., et al., 2019. Understanding the effects of formulation and process variables on the printlets quality manufactured by selective laser sintering 3D printing. Int. J. Pharm. 570, 118651 https://doi.org/10.1016/j.ijpharm.2019.118651.

Beitz, S., Uerlich, R., Bokelmann, T., Diener, A., Vietor, T., Kwade, A., 2019. Influence of powder deposition on powder bed and specimen properties. Materials 12 (2), 297. https://doi.org/10.3390/ma12020297.

Charoo, N.A., Barakh Ali, S.F., Mohamed, E.M., et al., 2020. Selective laser sintering 3D printing - An overview of the technology and pharmaceutical applications. Drug Dev. Ind. Pharm. 46 (6), 869–877. https://doi.org/10.1080/03639045.2020.1764027.

Chatterjee, B., Reddy, A., Santra, M., Khamanga, S., 2022. Amorphization of drugs for transdermal delivery-A recent update. Pharmaceutics 14 (5), 983. https://doi.org/10.3390/pharmaceutics14050983.

Cheah, C.M., Leong, K.F., Chua, C.K., Low, K.H., Quek, H.S., 2002. Characterization of microfeatures in selective laser sintered drug delivery devices. Proc. Inst. Mech. Eng. H: J. Eng. Med. 216 (6), 369–383. https://doi.org/10.1243/095441102321032166.

Coe, H.G., Pasebani, S., 2020. Use of bimodal particle size distribution in selective laser melting of 316L stainless steel. J. Manuf. Mater. Process. 4 (1), 8. https://doi.org/10.3390/jmmp4010008.

Davis Jr, D.A., Thakkar, R., Su, Y., Williams 3rd, R.O., Maniruzzaman, M., 2021. Selective laser sintering 3-dimensional printing as a single step process to prepare amorphous solid dispersion dosage forms for improved solubility and dissolution rate. J. Pharm. Sci. 110 (4), 1432–1443. https://doi.org/10.1016/j.xphs.2020.11.012.

Ettema Gerrit Jan Bouke, Jacobus Maria Lemmens, Theodorus Hendricus Antonius Peters, and Frantisek Picha. 2005. Zolpidem salts. EP 1,163,241 B1, filed March 13, 2000, and issued June 15, 2005.

Farzadfar, S.A., Murtagh, M.J., Venugopal, N., 2020. Impact of IN718 bimodal powder size distribution on the performance and productivity of laser powder bed fusion additive manufacturing process. Powder Technol. 375, 60–80. https://doi.org/10.1016/j.powtec.2020.07.092.

Fina, F., Goyanes, A., Gaisford, S., Basit, A.W., 2017. Selective laser sintering (SLS) 3D printing of medicines. Int. J. Pharm. 529 (1–2), 285–293. https://doi.org/10.1016/j.ijpharm.2017.06.082.

Fina, F., Madla, C.M., Goyanes, A., Zhang, J., Gaisford, S., Basit, A.W., 2018a. Fabricating 3D printed orally disintegrating printlets using selective laser sintering. Int. J. Pharm. 541 (1–2), 101–107. https://doi.org/10.1016/j.ijpharm.2018.02.015.

Fina, F., Goyanes, A., Madla, C.M., et al., 2018b. 3D printing of drug-loaded gyroid lattices using selective laser sintering. Int. J. Pharm. 547 (1–2), 44–52. https://doi.org/10.1016/j.ijpharm.2018.05.044.

Gaurav, H.N., Malik, A.K., et al., 2021. Recent update of 3D printing technology in pharmaceutical formulation development. J. Biomater. Sci. Polym. Ed. 32 (17), 2306–2330. https://doi.org/10.1080/09205063.2021.1967702.

Goodridge, R.D., Tuck, C.J., Hague, R.J.M., 2012. Laser sintering of polyamides and other polymers. Prog. Mater. Sci. 57 (2), 229–267. https://doi.org/10.1016/j.pmatsci.2011.04.001.

Gueche, Y.A., Sanchez-Ballester, N.M., Cailleaux, S., Bataille, B., Soulairol, I., 2021. Selective Laser Sintering (SLS), a new chapter in the production of Solid Oral Forms (SOFs) by 3D printing. Pharmaceutics 13 (8), 1212. https://doi.org/10.3390/pharmaceutics13081212.

Hamed, R., Mohamed, E.M., Rahman, Z., Khan, M.A., 2021. 3D-printing of lopinavir printlets by selective laser sintering and quantification of crystalline fraction by XRPD-chemometric models. Int. J. Pharm. 592, 120059 https://doi.org/10.1016/j.ijpharm.2020.120059.

Henry, S., De Vadder, L., Decorte, M., et al., 2021. Development of a 3D-printed dosing platform to aid in zolpidem withdrawal therapy. Pharmaceutics 13 (10), 1684. https://doi.org/10.3390/pharmaceutics13101684.

ISO/ASTM DIS 52910(en), Additive manufacturing — Design — Requirements, guidelines and recommendations, (n.d.). Accessed February 6, 2024. Available from: https://www.iso.org/obp/ui/#iso:std:iso-astm:52910:dis:ed-2:v1:en.

Kopp, S.P., Medvedev, V., Tangermann-Gerk, K., et al., 2023. Electrophotographic 3D printing of pharmaceutical films. Addit. Manuf. 73, 103707 https://doi.org/10.1016/j.addma.2023.103707.

Kulinowski P, Malczewski P, Łaszcz M, et al. Development of Composite, Reinforced, Highly Drug-Loaded Pharmaceutical Printlets Manufactured by Selective Laser Sintering-In Search of Relevant Excipients for Pharmaceutical 3D Printing. Materials (Basel). 2022;15(6):2142. Published 2022 Mar 14. doi:10.3390/ma15062142.

Kulinowski, P., Malczewski, P., Pesta, E., et al., 2021. Selective laser sintering (SLS) technique for pharmaceutical applications – Development of high dose controlled release printlets. Addit. Manuf. 38 (2), 101761 https://doi.org/10.1016/j.addma.2020.101761.

Kumar S. Selective Laser Sintering/Melting, in: Hashmi S, J. VTC, Batalha GF, Yilbas B (Eds.), Comprehensive Materials Processing. Elsevier, Amsterdam, 2014, pp. 93–134. doi:10.1016/B978-0-08-096532-1.01003-7.

Leong KF, Chua CK, Gui WS, Verani. Building porous biopolymeric microstructures for controlled drug delivery devices using selective laser sintering. Int. J. Adv. Manuf. Technol. 2006; 31(5-6): 483-489. doi: 10.1007/s00170-005-0217-4.

Levine V, Tikhomirov E, Lindh J, Quodbach J, Kipping T, editors. Investigation of Polymers for SLS 3D-Printing of Solid Oral Dosage Forms [Internet]. Boston: Springer Publishing Company; 2022. Available from: http://urn.kb.se/resolve?urn=urn:nbn:se:uu:diva-489833.

Lexow, M.M., Drummer, D., 2016. New materials for SLS: The use of antistatic and flow agents. J. Powder Technol. 1–9 https://doi.org/10.1155/2016/4101089.

Lim, S.H., Kathuria, H., Tan, J.J.Y., Kang, L., 2018. 3D printed drug delivery and testing systems - A passing fad or the future? Adv. Drug Deliv. Rev. 132, 139–168. https://doi.org/10.1016/j.addr.2018.05.006.

Maclean, N., Walsh, E., Soundaranathan, M., et al., 2021. Exploring the performance-controlling tablet disintegration mechanisms for direct compression formulations. Int. J. Pharm. 599, 120221 https://doi.org/10.1016/j.ijpharm.2021.120221.

Madžarević, M., Medarević, Đ., Pavlović, S., Ivković, B., Đuriš, J., Ibrić, S., 2021. Understanding the effect of energy density and formulation factors on the printability and characteristics of SLS Irbesartan tablets-application of the decision tree model. Pharmaceutics 13 (11), 1969. https://doi.org/10.3390/pharmaceutics13111969.

Mohamed, E.M., Barakh Ali, S.F., Rahman, Z., et al., 2020. Formulation optimization of selective laser sintering 3D-printed tablets of clindamycin palmitate hydrochloride by response surface methodology. AAPS PharmSciTech 21 (6), 232. https://doi.org/10.1208/s12249-020-01775-0.

Olakanmi, E.O., Cochrane, R.F., Dalgarno, K.W., 2015. A review on selective laser sintering/melting (SLS/SLM) of aluminium alloy powders: Processing, microstructure, and properties. Prog. Mater. Sci. 74, 401–447. https://doi.org/10.1016/j.pmatsci.2015.03.002.

Osei-Yeboah, F., Sun, C.C., 2015. Validation and applications of an expedited tablet friability method. Int. J. Pharm. 484 (1–2), 146–155. https://doi.org/10.1016/j.ijpharm.2015.02.061.

Padmakumar, M., 2020. Additive manufacturing of tungsten carbide hardmetal parts by Selective Laser Melting (SLM), Selective Laser Sintering (SLS) and Binder Jet 3D Printing (BJ3DP) techniques. Lasers Manuf. Mater. Process. 7, 338–371. https://doi.org/10.1007/s40516-020-00124-0.

Palo, M., Holländer, J., Suominen, J., Yliruusi, J., Sandler, N., 2017. 3D printed drug delivery devices: Perspectives and technical challenges. Expert Rev. Med. Devices 14 (9), 685–696. https://doi.org/10.1080/17434440.2017.1363647.

Paraiso, R.L.M., Rose, R.H., Fotaki, N., McAllister, M., Dressman, J.B., 2020. The use of PBPK/PD to establish clinically relevant dissolution specifications for zolpidem immediate release tablets. Eur. J. Pharm. Sci. 155, 105534 https://doi.org/10.1016/j.ejps.2020.105534.

Prajapati, S.T., Patel, A.N., Patel, C.N., 2011. Formulation and evaluation of controlled-release tablet of zolpidem tartrate by melt granulation technique. ISRN Pharm. 2011, 208394 https://doi.org/10.5402/2011/208394.

Sadeghi, F., Kamali, H., Kouhestanian, S., Hadizadeh, F., Nokhodchi, A., Afrasiabi, G.H., 2022. Supercritical CO2 versus water as an antisolvent in the crystallization process to enhance dissolution rate of curcumin. Pharm. Dev. Technol. 27 (10), 999–1008. https://doi.org/10.1080/10837450.2022.2143526.

Seoane-Viaño, I., Pérez-Ramos, T., Liu, J., et al., 2023. Visualizing disintegration of 3D printed tablets in humans using MRI and comparison with in vitro data. J. Control. Release. 365, 348–357. https://doi.org/10.1016/j.jconrel.2023.11.022.

Shirazi, S.F., Gharehkhani, S., Mehrali, M., et al., 2015. A review on powder-based additive manufacturing for tissue engineering: selective laser sintering and inkjet 3D printing. Sci. Technol. Adv. Mater. 16 (3), 033502 https://doi.org/10.1088/1468-6996/16/3/033502.

Souto, E.B., Campos, J.C., Filho, S.C., et al., 2019. 3D printing in the design of pharmaceutical dosage forms. Pharm. Dev. Technol. 24 (8), 1044–1053. https://doi.org/10.1080/10837450.2019.1630426.

Stanojević, G., Medarević, D., Adamov, I., Pešić, N., Kovačević, J., Ibrić, S., 2020. Tailoring atomoxetine release rate from DLP 3D-printed tablets using artificial neural networks: Influence of tablet thickness and drug loading. Molecules 26 (1), 111. https://doi.org/10.3390/molecules26010111.

Sun, C.C., Hou, H., Gao, P., Ma, C., Medina, C., Alvarez, F.J., 2009. Development of a high drug load tablet formulation based on assessment of powder manufacturability: moving towards quality by design. J. Pharm. Sci. 98 (1), 239–247. https://doi.org/10.1002/jps.21422.

Sweetman, S.C., 2009. Martindale: the complete drug reference Vol. 1, 1038.

Tabriz AG, Gonot-Munck Q, Baudoux A, et al. 3D Printing of Personalised Carvedilol Tablets Using Selective Laser Sintering. Pharmaceutics. 2023;15(9):2230. Published 2023 Aug 29. doi:10.3390/pharmaceutics15092230.

Tanaka, S., Sakai, Y., 2023. Estimation of actual pore-size distribution by inverse analysis of mercury intrusion. Constr. Build. Mater. 336, 130208 https://doi.org/10.1016/j.conbuildmat.2022.130208.

Thakkar, R., Zhang, Y., Zhang, J., Maniruzzaman, M., 2021. Synergistic application of twin-screw granulation and selective laser sintering 3D printing for the development of pharmaceutical dosage forms with enhanced dissolution rates and physical properties. Eur. J. Pharm. Biopharm. 163, 141–156. https://doi.org/10.1016/j.ejpb.2021.03.016.

The United States Pharmacopeia, 44th ed.; US Pharmacopeia Convention: Rockville, Maryland, 2021.

Tikhomirov, E., Åhlén, M., Di Gallo, N., et al., 2023. Selective laser sintering additive manufacturing of dosage forms: Effect of powder formulation and process parameters on the physical properties of printed tablets. Int. J. Pharm. 635, 122780 https://doi.org/10.1016/j.ijpharm.2023.122780.

Tikhomirov E. Selective laser sintering for 3D printing of medications [Internet] [PhD dissertation]. [Uppsala]: Acta Universitatis Upsaliensis; 2023. (Digital Comprehensive Summaries of Uppsala Dissertations from the Faculty of Science and Technology). Available from: https://urn.kb.se/resolve?urn=urn:nbn:se:uu:diva-508655.

Tonello, R., Conradsen, K., Pedersen, D.B., Frisvad, J.R., 2023. Surface roughness and grain size variation when 3D printing polyamide 11 parts using selective laser sintering. Polymers 15 (13), 2967. https://doi.org/10.3390/polym15132967.

Trenfield, S.J., Awad, A., Madla, C.M., et al., 2019. Shaping the future: recent advances of 3D printing in drug delivery and healthcare. Expert Opin. Drug Deliv. 16 (10), 1081–1094. https://doi.org/10.1080/17425247.2019.1660318.

Trenfield, S.J., Xu, X., Goyanes, A., et al., 2022. Releasing fast and slow: Non-destructive prediction of density and drug release from SLS 3D printed tablets using NIR spectroscopy. Int. J. Pharm. X 5, 100148. https://doi.org/10.1016/j.ijpx.2022.100148.

Wang, J., Zhang, Y., Aghda, N.H., et al., 2021. Emerging 3D printing technologies for drug delivery devices: Current status and future perspective. Adv. Drug Deliv. Rev. 174, 294–316. https://doi.org/10.1016/j.addr.2021.04.019.

Wu, B., Zhu, K., Wang, F., et al., 2022. Development of PA6/GO microspheres with good processability for SLS 3D printing. Polym. Eng. Sci. 62 (5), 1700–1709. https://doi.org/10.1002/pen.25957.

Yang, Y., Xu, Y., Wei, S., Shan, W., 2021. Oral preparations with tunable dissolution behavior based on selective laser sintering technique. Int. J. Pharm. 593, 120127 https://doi.org/10.1016/j.ijpharm.2020.120127.

Yu, D.G., Li, J.J., Williams, G.R., Zhao, M., 2018. Electrospun amorphous solid dispersions of poorly water-soluble drugs: A review. J. Control. Release. 292, 91–110. https://doi.org/10.1016/j.jconrel.2018.08.016.

Zhang, Y., Wu, K., Yang, Z., Ye, G., 2022. A reappraisal of the ink-bottle effect and pore structure of cementitious materials using intrusion-extrusion cyclic mercury porosimetry. Cem. Concr. Res. 161, 106942 https://doi.org/10.1016/j.cemconres.2022.106942.